14th European Signal Processing Conference (EUSIPCO 2006), Florence, Italy, September 4-8, 2006, copyright by EURASIP

RESTORATION OF ASTROPHYSICAL IMAGES - THE CASE OF POISSON GAMMA DATA

Céline Theys and Henri Lantéri

Laboratoire Universitaire d'Astrophysique de Nice, CNRS/Université de Nice Sophia-Antipolis
Parc Valrose, 06108 Nice cedex 2, France
phone: + (33) 04 92 07 63 10, fax: + (33) 04 92 07 63 21, email: theys@unice.fr

ABSTRACT

Very recent technology proposes to acquire astrophysic data with L3CCD cameras in order to avoid the read-out noise due to the classical CCD acquisition. The physical process leading to the data has been previously described by a "Poisson Gamma" density. We propose to discuss the model and to derive an iterative algorithm for the deconvolution of such data. Some simulation results are given on synthetic astrophysic data pointing out the interest of L3CCD cameras for acquisition of very low intensity images.

1. INTRODUCTION

This paper deals with the restoration of astrophysical images. Generally and until today astrophysic objets were acquired using charge coupled devices (CCD) cameras, leading to an additive Gaussian read-out noise on the data. For very low intensities data, the variance of the read-out noise is of the same order than most of the intensities in the image leading to unrecoverable distorsion. Recently, low light level CCD (LLLCCD or L3CCD) have been developed. L3CCD's amplify the signal prior to the readout amplifier resulting in a subelectron effective readout noise. This combined with the high quantum efficiency make them very interesting as interferometric detectors. Here we propose to study the effect that using an L3CCD would have on image restoration.

A brief description of the physical process leading to the data in optical astronomy imagery is given in section 2. A Poisson Gamma model for the output of the L3CCD is discussed in section 3. The problem of restoring the object from the data is stated in section 4. Section 5 details the iterative algorithm used and its application to the model under interest. Finally, some numerical results are shown in the section 6.

2. OPTICAL ASTRONOMY IMAGERY

The light emanating from the object of interest propagates through a turbulent atmosphere and is focused onto the Charge Coupled Device (CCD or L3CCD) by an imperfect optical system that limits the resolution and introduces aberrations.

The overall effect of the atmosphere and optical system can be mathematically described by a convolution operation between the object x and the Point Spread Function (PSF) h of the whole system:

$$z(r,s) = h(r,s) \otimes x(r,s), \tag{1}$$

where r and s are spatial coordinates and $\otimes$ denotes the two-dimensional convolution. In each pixel of the sensor, the interaction between the incident photons and the photosensitive material of the camera, creates photoelectrons n in proportion to the number of photons plus extraneous electrons due to heat and bias effects. If this last effect is neglected, this photo-conversion process is characterized by a Poisson transformation of mean z:

$$n \sim \mathscr{P}(z). \tag{2}$$

In the case of CCD cameras, the detector is read by an electronic process which adds a white Gaussian read-out noise.

3. DISCRETIZED MODEL FOR THE L3CCD ACQUISITION

The discretization of the process leads to arrays and vectors and in the following, we use capital letters for $N \times N$ arrays and bold letters for $N \times 1$ vectors, subscript i denotes the pixel i of the image lexicographically ordered.

From the description of the physical process, a realization of the value of the image in the pixel i, n_i, is a Poisson variable of mean $(H\mathbf{x})_i$:

$$p(N_i = n_i) = \frac{(H\mathbf{x})_i^{n_i}}{n_i!} \exp(-H\mathbf{x})_i, \tag{3}$$

where H is the classical block Toeplitz matrix for the convolution matrix form and $\mathbf{x}$ is the object ordered lexicographically.

A theoretical model of the L3CCD output probability distribution has been recently given in [2]. In this case, the process amplifying the signal is stochastic in such a way that the Poisson process is seen through a Gamma law $(n_i, 1/G)$ giving a data y_i distributed following:

$$p(y_i|N_i = n_i) = \frac{y_i^{n_i-1} \exp(-y_i/G)}{\Gamma(n_i) G^{n_i}}, \qquad \text{for } n_i > 0 \tag{4}$$

the probability law for the data y_i including the Poisson process in then :

$$p(y_i|\mathbf{x}) = \sum_{n_i=1}^{\infty} \frac{(H\mathbf{x})^{n_i}}{n_i!} \exp(-H\mathbf{x})_i \frac{y_i^{n_i-1} \exp(-y_i/G)}{\Gamma(n) G^{n_i}} \qquad \text{for } n_i > 0 \tag{5}$$

where G is the mean gain of the L3CCD detector.

This probability law describing the behavior of the acquired data, given the object is incorrect for at least two reasons:

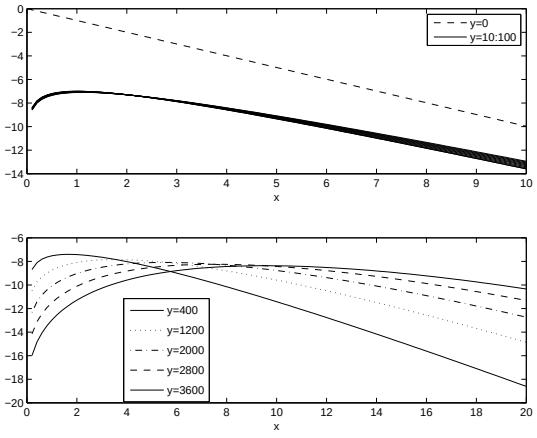

Figure 1: Log-likelihood $\log p(x_i|y_i)$ for $H = I$

- The first one is that the Gamma density is a continuous density while y_i, the data coming from the multiplication process, is necessarily an integer value. Analytic calculus of the normalization term for a "discrete Gamma distribution" is an open problem but it has been verified numerically .
- The second one is that the case $n_i = 0$ can not be included in the Gamma density but it must be put in eq. (5) to take into account the case of there is no photons in the pixel i giving obviously $y_i = 0$. Adding the corresponding density gives the final law:

$$p(y_i|\mathbf{x}) = \sum_{n_i=1}^{\infty} \frac{(H\mathbf{x})_i^{n_i}}{n_i!} \exp(-H\mathbf{x})_i \frac{y_i^{n_i-1}\exp(-y_i/G)}{\Gamma(n_i)G^{n_i}} + \exp(-H\mathbf{x})_i \delta_{y_i,0} \quad (6)$$

To give an idea of the behavior of this "Gamma Poisson" law, the simple case $H = I$, i.e for noisy data without convolution has been considered. In this case the value of y_i depends only of the value of x_i. Figure (1) shows the log-likelihood $\log p(x_i|y_i)$ with a mean gain G equals to 400. Figure 1(a) gives $\log p(x_i|y_i)$ for values of $y_i < G$, in this case the multiplication process is not really activated and the most probable value of x_i is 1 (except for $y = 0$ for which the most probable value is of course $x = 0$). For values of y_i superior to G, figure 1(b) , the maximum is moving to higher values of x and is approximately equal to y_i/G, underlining the multiplication process.

4. RECOVERING THE OBJECT FROM THE DATA

Problem of recovering $\mathbf{x}$ from $\mathbf{y}$ is a classical problem ill-posed in the sense of Hadamard. In the deconvolution problem for astronomical imaging the object is generally composed of bright objects on a sky background, assumed constant denoted by m. This particularity of the astrophysical object must be taken into account to avoid the "ringing" phenomena appearing in the vicinity of abrupt intensity variations. Moreover, in the convolution operation with normalized kernels, the total intensity of the object is maintained. The problem is then to restore the object $\mathbf{x}$ from the data $\mathbf{y}$ with the constraint $\mathbf{x} > m$ and the total intensity conservation, H being generally obtained via separated calibration measurements. A classical solution is to derive an iterative algorithm founded on the Maximum Likelihood Estimation (MLE).

From eq. (6) and with assumption of independence between pixels, the negative log-likelihood for the image is :

$$\begin{aligned} J(\mathbf{x}) &= -\sum_i \log p(y_i|\mathbf{x}) \\ &= -\sum_i \left[\sum_{n_i=1}^{\infty} \frac{z_i^{n_i}}{n_i!} \exp(-z_i) \frac{y_i^{n_i-1}\exp(-y_i/G)}{\Gamma(n_i)G^{n_i}} + \right. \\ &\quad \left. \exp(-z_i)\delta_{y_i,0} \right]. \end{aligned} \quad (7)$$

with $(H\mathbf{x})_i = z_i$. Then the MLE is obtained by minimizing $J(\mathbf{x})$ versus $\mathbf{x}$ with the lower bound and the intensity conservation constraints. The gradient of J, for the pixel i is:

$$(\nabla J(\mathbf{x}))_i = \sum_j (h_{ji} - h_{ji} r_j), \quad (8)$$

with h_{ji} the elements of the matrix H.

$$r_j = \frac{p_j}{q_j}, \quad (9)$$

$$p_j = \exp(-z_j)\exp(-y_j/G) \sum_{n_i} \frac{n_i y_j^{n-1} z_j^{n_i-1}}{n_i!\gamma(n_i)G_i^{n_i}} \quad (10)$$

and

$$q_j = \exp(-z_j)\exp(-y_j/G) \sum_{n_i} \frac{y_j^{n-1} z_j^{n_i}}{n_i!\gamma(n_i)G_i^{n_i}} + \exp(-z_j)\delta_{y_j,0} \quad (11)$$

We dont have analytic expressions for the series p_j and q_j but it can be easily seen that they are convergent.

The gradient vector can be expressed in the following matrix notation:

$$\nabla J(\mathbf{x}) = H^T \mathrm{diag}\left(\frac{1}{H\mathbf{x}}\right)(H\mathbf{x} - \mathbf{r}). \quad (12)$$

From this result, there is no explicit solution for the MLE of $\mathbf{x}$ and anyway it is well known that the MLE is not relevant for an ill-posed problem. A solution is to construct an iterative algorithm from the gradient and to stop the iterations before instability. The problem remains the determination of the optimal iterations number. A classical solution to circumvent this problem consists in regularizing the problem, i.e adding to the likelihood a term $J_2(\mathbf{x})$ with the aim of introducing to the solution a *prior* information, generally a smoothness property, [4], to stabilize the solution. The relative weight of the penalty versus the likelihood allows to "pull" the solution either towards the ML or towards the *prior*, changing the MLE in the Maximum A Posteriori (MAP) estimation and is tuned with a regularization parameter γ. The criterion to minimize becomes:

$$J_1(\mathbf{x}) + \gamma J_2(\mathbf{x}) \quad (13)$$

where $J_1(\mathbf{x})$ is given here by eq.(7). Even if the choice of the regularization function and the tuning of the regularization parameter exceed (for lack of space) the scope of this paper, we give in the sequel the iterative algorithm applied to the composite criterion 13.

5. THE ITERATIVE ALGORITHM

The MLE iterative algorithm can be easily obtained using the Split Gradient Method (SGM) previously proposed in various papers [6, 7, 9, 12].

5.1 SGM method

The regularized problem is to solve a problem of minimization under constraints, i.e:

- Minimize with respect to $\mathbf{x}$:

$$J(\mathbf{x},\gamma) = J_1(\mathbf{x}) + \gamma J_2(\mathbf{x}). \tag{14}$$

- With the constraints:
  1. Lower bound, $x_i - m \geq 0 \ \forall i$.
  2. Energy conservation, $\sum_i x_i = \sum_i y_i$.

Let us note that the considered functions $J_1(\mathbf{x})$ and $J_2(\mathbf{x})$ are convex. We propose to devise algorithms deduced from the Kuhn-Tucker (KT) conditions in the general modified gradient form [7, 6, 8].

$$x_i^{k+1} = C^k(x_i^k + \alpha_i^k f_i(\mathbf{x}^k,\gamma)(x_i^k - m)(-(\nabla J(\mathbf{x}^k,\gamma))_i). \tag{15}$$

The initial estimate $\mathbf{x}^0$ is chosen as a constant value, such that all the constraints are fulfilled, C^k is a normalization factor for the the total intensity conservation, subscript i is for the pixel i, $\alpha_i^k > 0$ is the relaxation factor, k is the iteration index, $f(\mathbf{x})$ is a function having positive values when $\mathbf{x}$ satisfies the constraints. To obtain "product form" algorithms, the split-gradient method (SGM) is used. It can be summarized as follows: the convex function $J(\mathbf{x}^k,\gamma)$ admits a finite unconstrained global minimum given by $\nabla J(\mathbf{x}^k,\gamma) = 0$, then we can write:

$$-\nabla J(\mathbf{x}^k,\gamma) = U(\mathbf{x}^k,\gamma) - V(\mathbf{x}^k,\gamma), \tag{16}$$

where $U(\mathbf{x}^k,\gamma)$ and $V(\mathbf{x}^k,\gamma)$ are two positive functions $\forall \mathbf{x}^k \geq m$. From (14), the total gradient can be decomposed as:

$$-\nabla J(\mathbf{x}^k,\gamma) = -\nabla J_1(\mathbf{x}^k) - \gamma \nabla J_2(\mathbf{x}^k). \tag{17}$$

Splitting $-\nabla J_1(\mathbf{x}^k)$ and $-\nabla J_2(\mathbf{x}^k)$ as in (16), we have

$$-\nabla J(\mathbf{x}^k,\gamma) = U_1(\mathbf{x}^k) - V_1(\mathbf{x}^k) + \gamma(U_2(\mathbf{x}^k) - V_2(\mathbf{x}^k)), \tag{18}$$

and

$$U(\mathbf{x}^k,\gamma) = U_1(\mathbf{x}^k) + \gamma U_2(\mathbf{x}^k), \tag{19}$$

$$V(\mathbf{x}^k,\gamma) = V_1(\mathbf{x}^k) + \gamma V_2(\mathbf{x}^k). \tag{20}$$

Taking:

$$f_i(\mathbf{x}^k,\gamma) = \frac{1}{V_i(\mathbf{x}^k,\gamma)} > 0, \tag{21}$$

eq. (15) becomes:

$$x_i^{k+1} = C^k\left(x_i^k + \alpha_i^k \frac{(x_i^k - m)}{V_i(\mathbf{x}^k,\gamma)}(U_i(\mathbf{x}^k,\gamma) - V_i(\mathbf{x}^k,\gamma))\right). \tag{22}$$

The maximum stepsize that ensures $x_i^{k+1} - m \geq 0, \forall i, \forall k$ is given by:

$$\alpha_m^k = \min_{i\in\mathscr{C}}\left(\frac{1}{1 - \frac{U_i(\mathbf{x}^k,\gamma)}{V_i(\mathbf{x}^k,\gamma)}}\right), \tag{23}$$

where $\mathscr{C}$ is the set of index i such that $(\nabla J(\mathbf{x}^k,\gamma))_i > 0$ and $x_i^k > m$; clearly $\alpha_m^k > 1$, then for $\alpha^k = 1$, the constraint is always fulfilled. The optimal step size α_c^k independent of i ensuring convergence must be computed in the range $]0,\alpha_m^k]$ (or $]0,\alpha_m^k[$ if a strict inequality constraint is required) by a line search procedure, (see for example [1, 3, 11, 10]), with the descent direction:

$$\boldsymbol{\rho}^k = \mathrm{diag}\left(\frac{(x_i^k - m)}{V_i(\mathbf{x}^k,\gamma)}\right)(U(\mathbf{x}^k,\gamma) - V(\mathbf{x}^k,\gamma)). \tag{24}$$

This direction is no more the negative gradient but it remains a descent direction for $J(\mathbf{x})$. The normalization i.e the computation of C^k is performed following [6]. To ensure the theoretical convergence of (22) without a dramatic increase of the computational cost, economic line search using the Armijo rule [1] or the Goldstein rule [5] can be used to compute α_c^k, as mentioned in [3].

5.2 Application to the Poisson Gamma model

The SGM algorithm has been applied to the Gamma Poisson model, without regularization, the gradient (eq. 12) is splitted into the functions U and V following:

$$U = H^T diag\left(\frac{1}{(H\mathbf{x})_i}\right)\mathbf{r} \qquad \text{and} \qquad V = 1 \tag{25}$$

$\sum_j h_{ji} = 1$ for normalized kernels. Finally, the estimated reconstructed object in the pixel i is at the iteration $k+1$:

$$\hat{x}_i^{k+1} = C^k\left(x_i^k + \alpha^k(x_i^k - m)((H^T\frac{\mathbf{r}.}{H\mathbf{x}})_i - 1)\right). \tag{26}$$

6. NUMERICAL ILLUSTRATIONS

6.1 Object

The proposed algorithm has been illustrated on a picture taken from the Hubble Space Telescope (HST) site, `http://hubblesite.org/gallery/`. It is a sun-like star nearing the end of its life, figure 2(a). A 128×128 subpicture has been extracted from the HST image, centered on the main structure, figure 2(c).

6.2 PSF

The data have been blurred with the normalized space invariant PSF, fig. 2(b). It is a realistic representation of the PSF of a ground based telescope including the effects of the atmospheric turbulence: the telescope aperture $P(r)$ is simply given by an array of points "1" inside a circle and "0" outside, the wavefront error $\delta(r)$ is an array of random numbers smoothed by a low-pass filter. The quantity $P(r)\exp\left(\frac{2i\pi\delta(r)}{\lambda}\right)$ represents the telescope aperture with the phase error; for the simulation, the peak to peak phase variation is small (less than π) and may correspond to typical telescope aberrations, see ([6]) for more details. The main interest of such a PSF simulation is that the Optical Transfer Function is a low pass filter, limited in spatial frequencies to the extent of the aperture auto correlation function, the blurred image, figure 2(d), is then strictly band limited corresponding to a realistic situation.

6.3 Some results

To stop the iterative procedure before noise amplification and/or to check the quality of the restoration process, we use a criterion based on the Euclidean distance $\varepsilon(k)$ between the true object $\mathbf{x}^*$ and the reconstructed one, computed as a function of k:

$$\varepsilon(k) = \frac{||\mathbf{x}^k - \mathbf{x}^*||}{||\mathbf{x}^*||}. \quad (27)$$

Such a comparison cannot be made for a real case since the true object is not known. However, it allows a good characterization of the behavior and performance of the algorithm for simulated data.

Fig. 3 shows a result in the case of data modeled by a Poisson Gamma density (L3CCD). Fig. 3(a) and (b) are the raw pictures respectively before and after amplification by a Gamma gain. Fig. 3(c) is the best result, in the sense of $\varepsilon(k)$ of the deconvolution algorithm, without regularization.

Fig. 4 compares image restoration with a CCD versus a L3CCD camera. Fig. 4(a) is a raw picture provided by a L3CCD with 1000 photons before the multiplication process while fig. 4(b) is a raw picture provided by a CCD with 1000 photons, corrupted by a read-out noise. In this case the result of the deconvolution algorithm is much better for the L3CCD, fig. 4(c) than for the CCD case, fig. 4(d).

7. CONCLUSION

An iterative reconstruction algorithm has been proposed to deconvolute Gamma Poisson data. First results on deconvolution of astrophysical images acquired with L3CCDs are given. These results compared with those obtained using data acquired with classical CCDs, underline the interest of such cameras in the case of very low intensity imagery.

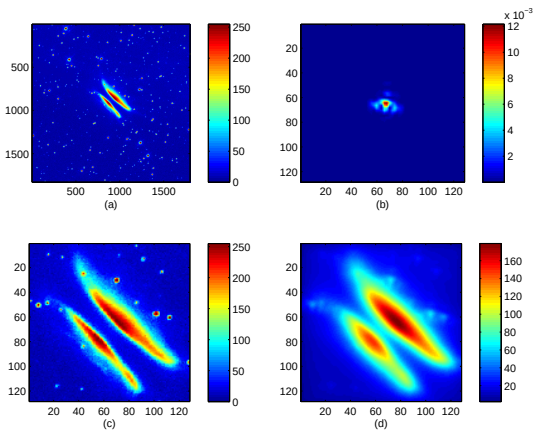

Figure 2: (a) Galaxy (b) Normalized PSF (c) Object (d) Result of the convolution

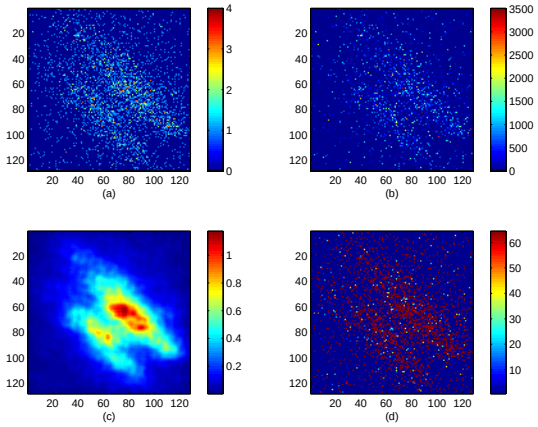

Figure 3: (a) Raw picture, 3000 photons (b) Raw picture + Gamma gain (c) $k_{min} = 2$, $\varepsilon_{min} = 0.44$ (d) Raw picture, other scale

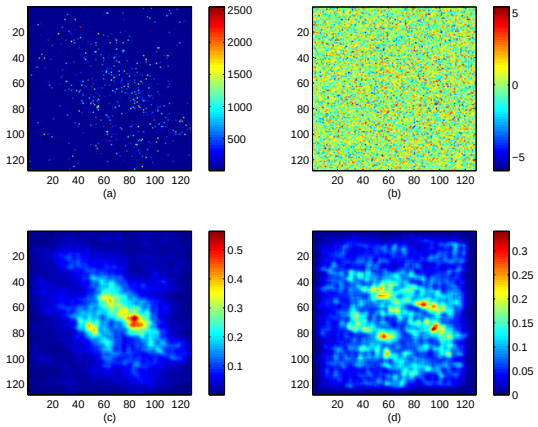

Figure 4: (a) Raw picture, 1000 photons + Gamma gain (b) Raw picture + Gaussian noise (c) $k_{min} = 6$, $\varepsilon_{min} = 0.45$ (d) $k_{min} = 5$, $\varepsilon_{min} = 0.68$

REFERENCES

[1] L. Armijo. Minimization of functions having continuous derivatives. *Pacific Journal of Mathematics*, (16):1–3, 1966.

[2] A. G. Basden and C. A. Haniff. Low light level ccds and visibility parameter estimation. *Mon. Not. R. Astron. Soc.*, 347:1187–1197, 2004.

[3] D. P. Bertsekas. *Non linear programming*. Athena Scientific, 1995.

[4] G. Demoment. Image reconstruction and restoration: Overview of common estimation structures and problems. *IEEE Transactions on ASSP*, 12(37):2024–2036, 1989.

[5] A. A Goldstein. *Constructive real analysis*. Harper New York, 1967.

[6] H. Lanteri, M. Roche, and C. Aime. Penalized maximum likelihood image restoration with positivity constraints- multiplicative algorithms. *Inverse problems*, 18:1397–1419, 2002.

[7] H. Lanteri, M. Roche, O. Cuevas, and C. Aime. A general method to devise maximum likelihood signal restoration multiplicative algorithms with non-negativity constraints. *Signal Processing*, 54(81):945–974, 2001.

[8] H. Lanteri, M. Roche, P. Gaucherel, and C. Aime. Ringing reduction in image reconstruction algorithms using a constraint on the inferior bound of the solution. *Signal Processing*, 82:1481–1504, 2002.

[9] H. Lanteri and C. Theys. Restoration of astrophysical images - the case of poisson data with additive gaussian noise. *Eurasip Journal on Applied Signal Processing - Special Issue on Applications of Signal Processing in Astrophysics and Cosmology*, (15):2500–2513, august 2005.

[10] D. G. Luenberger. *Introduction to linear and non linear programming*. Addison Wesley, Reading, Massachussets, 1973.

[11] Michel Minoux. *Programmation mathématique - Théorie et algorithmes*. Dunod, 1983.

[12] C. Theys and H. Lanteri. Restauration d'images dans le cas d'un bruit gaussien poissonnien. In *GRETSI*, 2005.